IEEE Access
Multidisciplinary | Rapid Review | Open Access Journal

Received April 7, 2021, accepted April 13, 2021, date of publication April 21, 2021, date of current version April 29, 2021.

Digital Object Identifier 10.1109/ACCESS.2021.3074786

Efficient Planar Near-Field Measurements for Radiation Pattern Evaluation by a Warping Strategy

MARIA ANTONIA MAISTO[1,2], GIOVANNI LEONE[1,2], (Member, IEEE), ADRIANA BRANCACCIO[1,2], (Member, IEEE), AND RAFFAELE SOLIMENE[1,2,3], (Senior Member, IEEE)

[1]Department of Engineering, Universitá degli Studi della Campania Luigi Vanvitelli, 81031 Aversa, Italy
[2]Consorzio Nazionale Interuniversitario per le Telecomunicazioni, 43124 Parma, Italy
[3]Department of Electrical Engineering, Indian Institute of Technology Madras, Chennai 600036, India

Corresponding author: Maria Antonia Maisto (mariaantonia.maisto@unicampania.it)

This work was supported by the Italian Ministry of University and Research through the PON Initiative under the Project Leonardo 4.0.

ABSTRACT The sampling of the near-field radiated by a planar source observed over a finite planar aperture is addressed. To this end, we employ the *warping* method that amounts to properly change the observation variables and finding the sampling points as those that allow to approximate the singular values of the radiation operator up to the so-called *number of degrees of freedom*. In particular, the warping transformations allow to approximate the kernel function of the relevant operator as a band-limited function and hence the sampling theorem is adopted to devise the discretization scheme. Here, we generalize the warping method to the full vector case and introduce a spatially varying oversampling strategy that allows to deal with measurement apertures which are larger than the source. It is shown that the sampling points need to be non-uniformly arranged across the measurement aperture but their number is generally much lower than classical half-wavelength sampling. A numerical analysis is included to support the theoretical arguments. Finally, numerical experiment-based results concerning the radiation pattern estimation of a planar array antenna are presented. To this end, experimental data collected under a uniform half-wavelength sampling scheme are first interpolated over the required non-uniform grid and then processed to obtain the radiation pattern.

INDEX TERMS Antenna measurements, near-field far-field (NFFF) transformation, sampling methods, antenna radiation patterns, non-uniform sampling.

I. INTRODUCTION

Near-field techniques [1], [2] have become a standard tool in antenna testing because of their high reliability. They basically consist in collecting near-field measurements and then, in order to evaluate the radiation pattern, processing them by some near-field to far-field transformations [2]–[6].

In this paper, we are concerned with planar measurement systems. In this case, a probe usually scans the measurement aperture with a sampling step of half the free-space wavelength [7]. Such a spatial step complies with the plane-wave spectrum bandwidth within the so-called visible domain. Also, the resulting uniform sampled data naturally match the input required by standard FFT algorithms which are used to compute the corresponding radiation pattern. However, this strategy can lead to a large number of measurement points, depending on the electric size (in terms of the wavelength) of the measurement aperture, which in turn depends on the radiating system size. Of course, this badly affects the overall time required to perform the antenna testing, especially when on-the-fly acquisition cannot be accepted, due to the complexity of the radiating system. For instance, for an advanced multi-beam radar, the probe has to stop at each measurement position to test a great deal of sum and difference beams which point at different directions in a large angular sector, within the whole operation frequency band.

The associate editor coordinating the review of this manuscript and approving it for publication was Shah Nawaz Burokur.

Therefore, the question of reducing the number of spatial measurements naturally arises and has theoretical and practical interest [8]–[10].

The mathematical rationale which entitles to look for a data reduction, with respect to the half-wavelength sampling strategy, is the compactness of the radiation operator [11]. Roughly speaking, compactness entails that the range of the radiation operator, that is the set of radiated fields, can be approximated by a finite dimensional space whose dimension depends, in general, on the required degree of accuracy [12]. In particular, since the probe and the antenna under test are usually located a few wavelengths apart to reduce coupling, the singularity of the Green function, which is the kernel of the radiation operator, is avoided. Therefore, such a kernel behaves nearly as an entire function of exponential type [13]. This leads the singular values of the radiation operator to nearly exhibit a step-like behaviour, i.e., they abruptly decay, according to an exponential law, beyond a certain critical index. The latter is the so-called number of degrees of freedom (NDF) of the radiated field and identifies the dimension of the field space. The NDF, of course, depends on the geometrical configuration parameters. However, for compactly supported sources, the NDF is always finite, even for unbounded observation domains [14], and, what is more, it is lower (sometimes much lower) than the number of measurement points required by the half-wavelength sampling. More in detail, by *only* assuming that the source has bounded energy (i.e., the source current is a square integrable function), then the *first* NDF singular functions provide an extremal set, i.e., the one of dimension equal to the NDF which yields the lowest representation error [15]. Accordingly, finding the sampling strategy can be cast as the determination of the nodes of some interpolation scheme which best approximates such a space.

From a general perspective, devising the sampling scheme can be addressed by a sensor selection procedure [16]. This way, the problem is phrased as the search for a finite number of measurement positions, among candidates available over a dense grid, by optimizing some metrics related to the singular values of the radiation operator [17]–[21]. Another approach takes into account the mathematical features of the Green function that suggests the field can be approximated by a band-limited function, once a suitable parametrization for the observation variables is employed and a proper demodulating exponential term is singled-out [22]. As a consequence, the field can be approximated by a sampling expansion and the measurement points are set accordingly.

Recently, we have introduced an approach that is somehow in between the two mentioned ones. Basically, we cast the determination of the sampling points as the ones that allow to approximate the kernel function of the operator consisting of the composition of the radiation operator and its adjoint [23]. In particular, thanks to suitable variable transformations, that *warp* the spatial observation variables, such a kernel function is approximated as a band-limited function and then the Shannon sampling theorem is used for the discretization. This method, unlike sensor selection procedures, does not require to run iterative optimization algorithms. Also, it generalizes the point of view of band-limited approximation approaches, since it does not require splitting the 2D problem into two 1D problems, along the so-called meridian and azimuth curves, since the outset. Indeed, it was shown that the sampling can be factorized (i.e., independently achieved along each dimension) only when the size of the measurement aperture is at most equal to the one of the source [23].

Unfortunately, in order to control the truncation error while estimating the radiation pattern, measurement apertures are often larger than the source. In these cases, the factorized approach tends to under-sample the aperture regions that are beyond the size of the source. To cope with this issue, suitable warping transformations can be determined, which is a feasible but actually complex task. Therefore, one can still consider using the factorized approach by introducing an oversampling factor that allows for a finer grid of points. This, however, decreases the amount of data that can be saved (as compared to the half-wavelength sampling) and leads to oversampling part of the measurement aperture that actually does not need that.

The first contribution of this paper is the generalization of the warping procedure, that in [23] has been derived only for magnetic source currents, to any type of currents. In particular, in the case of electric currents, there are some further technical difficulties to be tackled.

Secondly, we aim at introducing a simple method to find a balance between the more complex warping transformations and the need for oversampling. In particular, we propose a simple procedure in which the oversampling factor is set according to a spatially varying law. The very basic idea is to increase the sample density only where it is needed by the factorized approach.

Finally, the warping approach is validated by computing the radiation pattern (both the sum and the difference ones) of a planar array antenna of a tracking radar. It is shown that the warping approach requires much fewer sampling points than the ones required by the half-wavelength sampling (our benchmark). In this regard, we point out that the experimental data collected under a uniform $\lambda/2$ scheme are first interpolated over the required non-uniform grid and then processed.

The rest of the paper is organized as follows. Section II is devoted to giving the mathematical description of the problem and of the warping method. In Section III the spatially varying oversampling strategy is detailed, whereas Section IV reports the sampling scheme validation. Finally, Conclusions end the paper.

II. PROBLEM FORMULATION AND THE WARPING APPROACH

In this section, we introduce the mathematical formulation and the related notation to be used throughout the paper. Also, the field sampling scheme based on the warping transformations, presented in [23], is briefly detailed in order to establish the starting point from which to proceed ahead.

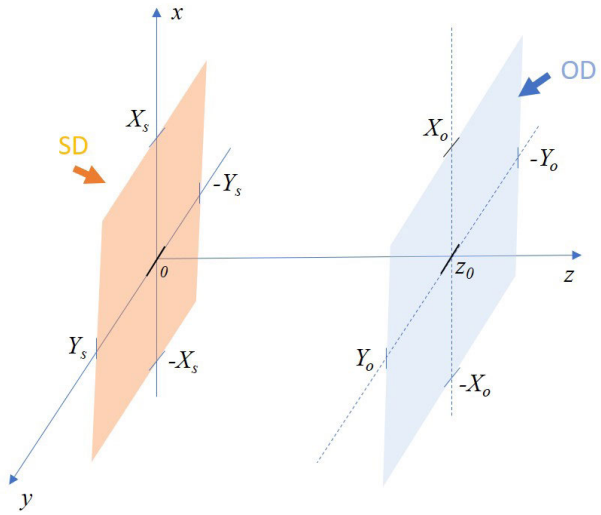

FIGURE 1. Geometry of the problem.

A. MATHEMATICAL FORMULATION

Consider a planar current $\mathbf{J}$ (electric or magnetic) spatially supported over $SD = [-X_s, X_s] \times [-Y_s, Y_s]$ (i.e., the source domain) located at $z = 0$. The source domain, being finite and planar, naturally fits the case that the transmitting antenna is a planar array. The radiated field is measured over a planar observation domain, $OD = [-X_0, X_0] \times [-Y_0, Y_0]$, located in front of the source at $z = z_o$ (see Fig. 1). We assume to work at single frequency, ω, with the time dependence understood as $e^{j\omega t}$.

The radiated field is linked to the radiating source through the following radiation operator,

$$\mathcal{G} : \mathbf{J} \in L^2(SD^3) \rightarrow \mathbf{E}(\mathbf{r}_o) = \int_{SD} \underline{G}(\mathbf{r}_o, \mathbf{r}) \cdot \mathbf{J}(\mathbf{r}) d\mathbf{r} \in L^2(OD^2)) \quad (1)$$

where $\mathbf{r}_o \in OD$, $\underline{G}(\mathbf{r}_o, \mathbf{r})$ is the free-space dyadic Green function (electric or magnetic depending on the type of the source under concern) and $\cdot$ denotes the inner product. It is noted that all the vector functions are assumed to belong to square integrable functional sets. In particular, $\mathbf{E} \in L^2(OD^2)$ means that only the two tangential field components are considered. Also, we remark that in (1) the probe response has not been considered. Probe antennas usually have a wide plane-wave spectrum, hence their effects can be considered negligible. Moreover, as argued in literature [24], the measurement operator can introduce a further smoothing on the field data.

B. WARPING METHOD

In order to devise the sampling scheme, in [23] we considered finding a discrete approximation of the following eigenvalue problem

$$(\mathcal{G}\mathcal{G}^\dagger \mathbf{u}_n)(\mathbf{r}_o) = \sigma_n^2 \mathbf{u}_n(\mathbf{r}_o) \quad (2)$$

with $\mathcal{G}^\dagger$ being the adjoint of $\mathcal{G}$ and σ_n^2 and $\mathbf{u}_n$ the relevant n-th eigenvalue (i.e., the squared singular value) and eigenfunction. In particular, the kernel function of the operator in (2) is given by

$$\underline{K}(\mathbf{r}_o, \mathbf{r}'_o) = \int_{SD} \underline{G}(\mathbf{r}_o, \mathbf{r}) \cdot \underline{G}^H(\mathbf{r}'_o, \mathbf{r}) d\mathbf{r} \quad (3)$$

where ^{H} means conjugation and transposition and $\underline{K}(\mathbf{r}_o, \mathbf{r}'_o)$ is a 2×2 matrix of functions, since only the field tangential components are assumed to be collected. Once the exponential term of the Green function is singled-out, its n, m entry can be written as

$$K_{n,m}(\mathbf{r}_o, \mathbf{r}'_o) = \int_{SD} H_{n,m}(\mathbf{r}_o, \mathbf{r}'_o, \mathbf{r}) e^{j[\Phi(\mathbf{r}_o, \mathbf{r}) - \Phi(\mathbf{r}'_o, \mathbf{r})]} d\mathbf{r} \quad (4)$$

where $H_{n,m}(\mathbf{r}_o, \mathbf{r}'_o, \mathbf{r})$ are the amplitude terms whereas $\Phi(\mathbf{r}_o, \mathbf{r}) = k|\mathbf{r}_o - \mathbf{r}|$ and k is the free-space wavenumber. The main idea of the warping method is to recast the phase term as

$$\Phi(\mathbf{r}_o, \mathbf{r}) - \Phi(\mathbf{r}'_o, \mathbf{r}) = \int_{\nu_0}^{\nu_1} \nabla_{\mathbf{p}} \Phi(\mathbf{p}(\nu), \mathbf{r},) \frac{d\mathbf{p}(\nu)}{d\nu} d\nu \quad (5)$$

where $\nabla_{\mathbf{p}}$ denotes the gradient with respect to $\mathbf{p}$ and $\mathbf{p}(\nu)$ is a curve whose starting and ending points coincide with $\mathbf{r}'_o$ and $\mathbf{r}_o$, respectively. The curve $\mathbf{p}(\nu)$ can be conveniently chosen to let the phase term resemble a Fourier kernel. For example, in [23], we considered a polygonal line with nodes in $\mathbf{r}'_o = (x'_o, y'_o)$, $\tilde{\mathbf{r}}_o = (x_o, y'_o)$ and $\mathbf{r}_o = (x_o, y_o)$. Accordingly,

$$\Phi(\mathbf{r}_o, \mathbf{r}) - \Phi(\mathbf{r}'_o, \mathbf{r}) = \mathbf{w}(\mathbf{r}_o, \mathbf{r}'_o, \mathbf{r}) \cdot (\mathbf{r}_o - \mathbf{r}'_o) \quad (6)$$

with $\mathbf{w} = (w_x, w_y)$ given by

$$w_x(x_o, \mathbf{r}'_o, \mathbf{r}) = \int_0^1 \left. \frac{\partial \Phi(p_x, y'_o, \mathbf{r},)}{\partial p_x} \right|_{p_x = x'_o + \nu(x_o - x'_o)} d\nu \quad (7)$$

$$w_y(\mathbf{r}_o, y'_o, \mathbf{r}) = \int_0^1 \left. \frac{\partial \Phi(x_o, p_y, \mathbf{r})}{\partial p_y} \right|_{p_y = y'_o + \nu(y_o - y'_o)} d\nu \quad (8)$$

Since the transformation $\mathbf{w} : \mathbf{r} \rightarrow \mathbf{w}(\mathbf{r}_o, \mathbf{r}'_o, \mathbf{r})$ is injective and the corresponding Jacobian matrix full rank $\forall \mathbf{r}_o, \mathbf{r}'_o$, (4) can be rewritten as

$$K_{n,m}(\mathbf{r}_o, \mathbf{r}'_o) = \int_{\Omega(\mathbf{r}_o, \mathbf{r}'_o)} \tilde{H}_{n,m}(\mathbf{r}_o, \mathbf{r}'_o, \mathbf{w}) e^{j\mathbf{w} \cdot (\mathbf{r}_o - \mathbf{r}'_o)} d\mathbf{w} \quad (9)$$

where

$$\Omega(\mathbf{r}_o, \mathbf{r}'_o) = \{(w_x(x_o, \mathbf{r}'_o, \mathbf{r}), w_y(\mathbf{r}_o, y'_o, \mathbf{r})) : \mathbf{r} \in SD\} \quad (10)$$

is the corresponding integration domain under the $\mathbf{w}$ variable and $\tilde{H}_{n,m}(\mathbf{r}_o, \mathbf{r}'_o, \mathbf{w})$ includes the Jacobian determinant associated to the adopted transformation.

Eq. (9) highlights the kernel functions somehow as spatially varying band-limited functions with band given by $\Omega(\mathbf{r}_o, \mathbf{r}'_o)$. In general, $\Omega(\mathbf{r}_o, \mathbf{r}'_o)$ does not have a canonical shape. However, one can simplify a little bit the matter by considering the smallest rectangular domain that includes it. Denote as $\Omega_R(\mathbf{r}_o, \mathbf{r}'_o) = \mathbf{w}_m(\mathbf{r}_o, \mathbf{r}'_o) + [-\Delta_{w_x}(\mathbf{r}_o, \mathbf{r}'_o), \Delta_{w_x}(\mathbf{r}_o, \mathbf{r}'_o)] \times [-\Delta_{w_y}(\mathbf{r_o}, \mathbf{r}'_o), \mathbf{r}'_o), \Delta_{w_y}(\mathbf{r_o}, \mathbf{r}'_o)]$ such a rectangular domain, with $\mathbf{w}_m(\mathbf{r}_o, \mathbf{r}'_o)$ being its

centre of mass. Accordingly, $w = w_m + \bar{w}$ and (9) can be rewritten as

$$K_{n,m}(\mathbf{r}_o, \mathbf{r}'_o) \simeq e^{j\mathbf{w}_m\cdot(\mathbf{r}_o-\mathbf{r}'_o)} \times \int_{-\Delta_{w_x}}^{\Delta_{w_x}} \int_{-\Delta_{w_y}}^{\Delta_{w_y}} \tilde{H}_{n,m}(\mathbf{r}_o, \mathbf{r}'_o, \mathbf{w}) e^{j\bar{\mathbf{w}}\cdot(\mathbf{r}_o-\mathbf{r}'_o)} d\bar{\mathbf{w}} \quad (11)$$

where the dependence on $(\mathbf{r}_o, \mathbf{r}'_o)$ of $\mathbf{w}_m$, Δ_{w_x} and Δ_{w_y} has been understood for the sake of notation simplicity.

The spatially varying nature of the bandwidth can be removed if the observation variables are properly warped. As shown in [23], this is quite simple when $OD \subseteq SD$, i.e., if the measurement aperture's size does not exceed the one of the source. In particular, in this case it has been shown that $\Delta_{w_x}(x_o, x'_o)$ and $\Delta_{w_y}(y_o, y'_o)$, that is the band edges, depend separately on the two observation Cartesian coordinates. This has suggested adopting the following transformations

$$\boldsymbol{\xi} : \mathbf{r}_o \to \boldsymbol{\xi} = (\xi_x, \xi_y) \quad (12)$$

with

$$\xi_x(x_o) = \frac{k}{2}\left[\sqrt{(x_o + X_s)^2 + z_o^2} - \sqrt{(x_o - X_s)^2 + z_o^2}\right]$$
$$\xi_y(y_o) = \frac{k}{2}\left[\sqrt{(y_o + Y_s)^2 + z_o^2} - \sqrt{(y_o - Y_s)^2 + z_o^2}\right]$$

and

$$\boldsymbol{\gamma} : (x_o, y_o) \to \boldsymbol{\gamma} = (\gamma_x, \gamma_y) \quad (13)$$

with

$$\gamma_x(x_o) = \frac{k}{2}\left[\sqrt{(x_o + X_s)^2 + z_o^2} + \sqrt{(x_o - X_s)^2 + z_o^2}\right]$$
$$\gamma_y(y_o) = \frac{k}{2}\left[\sqrt{(y_o + Y_s)^2 + z_o^2} + \sqrt{(y_o - Y_s)^2 + z_o^2}\right]$$

that allows to rearrange eq. (11) as

$$K_{n,m}(\mathbf{r}_o, \mathbf{r}'_o) \simeq e^{j[(\boldsymbol{\gamma}-\boldsymbol{\gamma}')\cdot(\hat{x}+\hat{y})]} \times \int_{-1}^{1} \int_{-1}^{1} \hat{H}_{n,m}(\boldsymbol{\xi}, \boldsymbol{\xi}', \hat{\mathbf{w}}) e^{j\hat{\mathbf{w}}\cdot(\boldsymbol{\xi}-\boldsymbol{\xi}')} d\hat{\mathbf{w}} \quad (14)$$

where $\hat{x}$ and $\hat{y}$ are Cartesian direction vectors, $\boldsymbol{\gamma} = \boldsymbol{\gamma}(\mathbf{r}_o)$, $\boldsymbol{\gamma}' = \boldsymbol{\gamma}(\mathbf{r}'_o)$, $\boldsymbol{\xi} = \boldsymbol{\xi}(\mathbf{r}_o)$, $\boldsymbol{\xi}' = \boldsymbol{\xi}(\mathbf{r}'_o)$, $\hat{w} = \bar{w} \cdot (1/\Delta_{w_x}, 1/\Delta_{w_y})$ and $\hat{H}_{n,m}(\boldsymbol{\xi}, \boldsymbol{\xi}', \hat{\mathbf{w}})$ now includes the scaling factor of the transformation from $\bar{w}$ to $\hat{w}$.

The case of magnetic currents was addressed in [23]. In such a case, the amplitude term $\hat{H}_{n,m}(\boldsymbol{\xi}, \boldsymbol{\xi}', \hat{\mathbf{w}})$ is very weakly dependent on $\boldsymbol{\xi}$ and $\boldsymbol{\xi}'$. Therefore, the kernel (14) is practically a band-limited function. As a consequence, the sampling approach can be used to obtain a finite dimensional approximation of $\mathcal{GG}^\dagger$ [25]. In particular, adapting the results reported in [25] to the case at hand, entails that the eigenfunctions, and hence the field components, can be expanded according to a sampling series (see [23] for the mathematical details). Thus, the n-th field component (i.e., along $\hat{x}$ or $\hat{y}$) can be expressed as

$$E_n(\xi_x, \xi_y) = e^{j\gamma_x(\xi_x)} e^{j\gamma_y(\xi_y)} \sum_{m,l} E_n(\xi_{xm}, \xi_{yl}) \times e^{-j\gamma_x(\xi_{xm})} e^{-j\gamma_y(\xi_{yl})} \mathrm{sinc}(\xi_x - \xi_{xm}) \mathrm{sinc}(\xi_y - \xi_{yl}) \quad (15)$$

where the sampling points are given by

$$\xi_{xm}(x_{om}) = m\pi$$
$$\xi_{yl}(y_{ol}) = l\pi \quad (16)$$

In (16), (x_{om}, y_{ol}) are the sampling points in the usual coordinates, and their indices run as long as they belong to the measurement aperture. Therefore, as we have pointed out in the introduction, (15) is actually a truncated series which is asked to approximate the field well as long as it belongs to the set spanned by the first NDF singular functions.

In the case of electric currents, $\hat{H}_{n,m}(\boldsymbol{\xi}, \boldsymbol{\xi}', \hat{\mathbf{w}})$ cannot be considered nearly constant with $\boldsymbol{\xi}$ and $\boldsymbol{\xi}'$. Nonetheless, the previous field expansion can still be considered to hold. This is because the amplitude term is usually a slowly varying function, so that the exponential factor actually plays the major role. This statement can actually be cast under more rigorous roots, as done in [26] for a scalar problem, by resorting to the pseudosampling series theory introduced by Horiuchi [27]. Indeed, according to [27], the kernel function in (14) admits a pseudosampling series expansion. This is not exactly a sampling expansion since the coefficients are not the function's samples but rather functions that depend on observation variable $\boldsymbol{\xi}$. However, since the latter ones are slowly variant functions, they can be approximated by their value around the function's sample and hence the classical sampling series structure is restored. These arguments have been thoroughly detailed in [26] and hence are not repeated here.

III. SPATIALLY VARYING OVERSAMPLING

According to previous arguments, the sampling points can be found by solving eqs. (16) for x_{om} and y_{ol}. Therefore, while the sampling is uniform along the warped variables ξ_x and ξ_y, it is actually non-uniform in the (x_o, y_o) domain. In particular, the sampling along x_o and y_o is factorized, that is it can be independently performed. As remarked, this is a consequence of the assumption $OD \subseteq SD$. However, the measurement aperture is often larger than the source in order to control the truncation error while computing the radiation pattern. Then, while previous developments can be still adopted, the warping transformations become more complex to be derived and the sampling scheme results no longer factorized.

To avoid this technical difficulty, one can use the same sampling as in (16) but, as noted in [23], the field in the spatial regions of OD which exceed the size of SD can be under-sampled. An obvious way to deal with this issue is to introduce a certain degree of oversampling. Oversampling, indeed, is generally beneficial since it allows to mitigate the truncation error due to the finiteness of the measurement aperture, and after all, it is in general required since the near-field is not exactly a band-limited function.

Accordingly, say $[-\Delta\xi_x, \Delta\xi_x] \times [-\Delta\xi_y, \Delta\xi_y]$ the observation domain in the warped domain, which corresponds to OD, and α_x and α_y the *uniform* oversampling factors along x and y, respectively, then the number of samples becomes

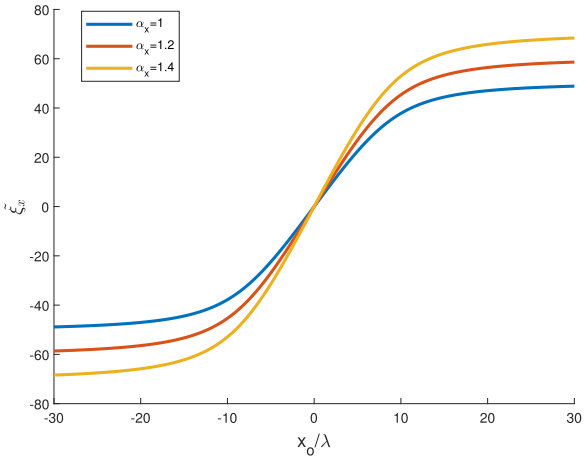

FIGURE 2. Behaviour of $\tilde{\xi}_x$ as a function of x_o for different values of uniform oversampling factor $\alpha_x \in \{1, 1.2, 1.4\}$. The geometrical parameters are $X_s = 8\lambda$, $Y_s = 4\lambda$, $X_0 = 30\lambda$, $Y_0 = 15\lambda$ and $z_o = 7\lambda$.

$N = N_x N_y$, with $N_x = [2\alpha_x \Delta\xi_x/\pi]$, $N_y = [2\alpha_y \Delta\xi_y/\pi]$ and $[\cdot]$ being the operator that takes the integer part.

The point is that a uniform oversampling strategy is not the best way to tackle the problem since it leads to an increased number of samples even for measurement aperture regions that are already properly sampled. An intuitive and more suited strategy is to devise the warping transformations in order to obtain a finer sampling grid only for the points (x_o, y_o) outside SD. This can be achieved by a non-uniform oversampling factor.

The previous arguments can be put into an algorithmic form by introducing new warping transformations as follows,

$$\begin{aligned} \tilde{\xi}_x &= \alpha_x(x_o)\xi_x \\ \tilde{\xi}_y &= \alpha_y(y_o)\xi_y \end{aligned} \tag{17}$$

from which the spatial sampling points can be found by solving

$$\begin{aligned} \tilde{\xi}_{xm}(x_{om}) &= m\pi \\ \tilde{\xi}_{yl}(y_{ol}) &= l\pi \end{aligned} \tag{18}$$

and hence (15) rewrites as

$$\begin{aligned} E_n(\tilde{\xi}_x, \tilde{\xi}_y) = e^{j\gamma_x(\tilde{\xi}_x)} e^{j\gamma_y(\tilde{\xi}_y)} \sum_{m,l} E_n(\tilde{\xi}_{xm}, \tilde{\xi}_{yl}) \\ \times e^{-j\gamma_x(\tilde{\xi}_{xm})} e^{-j\gamma_y(\tilde{\xi}_{yl})} \mathrm{sinc}(\tilde{\xi}_x - \tilde{\xi}_{xm}) \mathrm{sinc}(\tilde{\xi}_y - \tilde{\xi}_{yl}) \end{aligned} \tag{19}$$

If α_x and α_y are constant with respect to x_o and y_o, clearly (19) refers to a uniform oversampling. Fig. 2 depicts $\tilde{\xi}_x$ (similar behaviour of course occurs for $\tilde{\xi}_y$) for different degrees of uniform oversampling. As can be seen, the behaviour of the warping transformation is non-linear, which entails a non-uniform sampling in x_o. Moreover, the effect of the oversampling factor is to increase its slope and hence to reduce the sampling step, as required. However, even for low values of x_o (where the behaviour is nearly linear) there is a reduction of the sampling step, roughly of $1/\alpha_x$. Since in the latter region oversampling is not needed, a better way to set α_x is to allow it to be non-constant, i.e., $\alpha_x = \alpha_x(x_o)$, and assuming larger value for high x_o. While doing that, however, one must make sure that the resulting $\tilde{\xi}_x = \alpha_x(x_o)\xi_x$ and $\alpha_y = \alpha_y(y_o)$ are monotonic functions, which is necessary to uniquely pass from x_o and y_o to the warped variables. A possible simple choice for the oversampling factor, which complies with all the previous requirements, is for example

$$\alpha_x(x_o) = 1 - (1 - \nu)\sin^p\left(\frac{\pi}{2X_0} x_o\right) \tag{20}$$

which is a function ranging (within the measurement aperture) from 1 ($x_o = 0$) to ν ($x_o = X_0$) with the sin term and the parameter p controlling the transition. The behaviour of (20) along with the corresponding warping transformations are shown in Fig. 3. As can be seen, $\alpha_x(x_o)$ actually complies with the expected behaviour. In particular, in the next examples we will consider $p = 4$.

Finally, it is noted that for a given ν, since the intervals in $\tilde{\xi}_x$ (resp. $\tilde{\xi}_y$), as well as the sampling steps in the warped domains, are the same for both the uniform and the non-uniform oversampling strategies, the number of the required samples coincides: what changes is their deployment across the measurement aperture.

IV. SAMPLING SCHEME VALIDATION

In this section we apply the proposed data sampling scheme in order to verify its effectiveness. First, we run numerical simulations in order to appreciate if the proposed sampling scheme (both with uniform and non-uniform oversampling) succeeds in approximating the eigenvalues of $\mathcal{G}\mathcal{G}^\dagger$, for which it was actually conceived. Then, we address the radiation pattern estimation using measured data.

A. EIGENVALUE COMPUTATION

In order to compute the eigenvalues of $\mathcal{G}\mathcal{G}^\dagger$ we need to numerically solve eq. (2). To this end, the singular functions are expanded as in (19) so that the equivalent matrix version of $\mathcal{G}\mathcal{G}^\dagger$ is obtained. Say $\mathbf{G}_p^\nu$ the corresponding matrix, with p specified as above (in particular, $p = 0$ means uniform oversampling) and ν denotes the degree of oversampling. In general, according to the mathematical framework described above, $\mathbf{G}_p^\nu \in C^{2N\times 2N}$, with $N = N_x N_y$. For the sake of simplicity of computation, here we consider the case of a planar magnetic current having only x and y components. In such a case, the vector problem splits into two identical scalar problems and the corresponding discrete version of the pertinent operators is a matrix $\in C^{N\times N}$ [23].

The estimation of the eigenvalues of $\mathcal{G}\mathcal{G}^\dagger$ is shown in Fig. 4. In particular, panel (*a*) refers to the case $OD = SD$. As anticipated, in this case the sampling scheme in (16) (i.e., with $\nu = 1$ and hence without oversampling) already allows to approximate the eigenvalue behaviour very well, though it requires $N_{\nu=1} = 1764$ measurement points instead of $N_{\lambda/2} = 3136$ of the half-wavelength sampling. In panel (**b**) the measurement aperture is larger than SD and requires

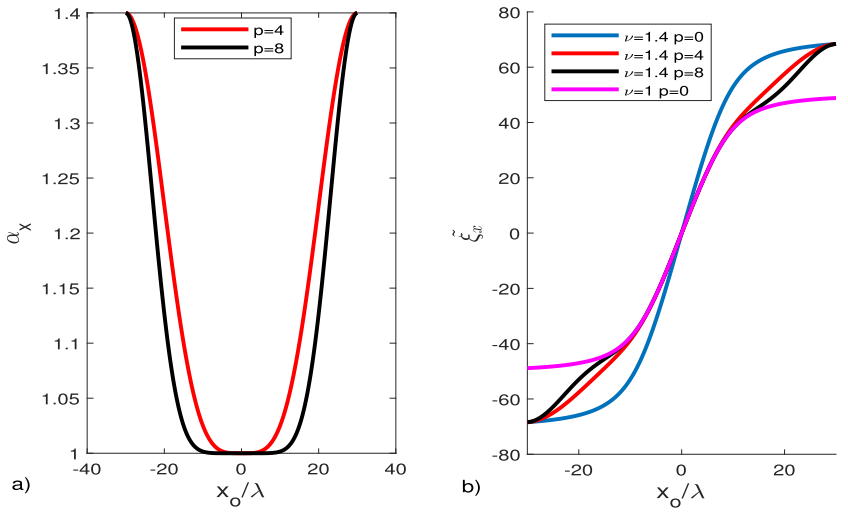

FIGURE 3. Illustrating the spatially varying oversampling due to (20). Panel a) shows the behaviour of α_x in terms of x_o for different values of p and $\nu = 1.4$, whereas panel b) reports the behaviour of $\tilde{\xi}_x$. The geometrical parameters are the same as Fig. 2.

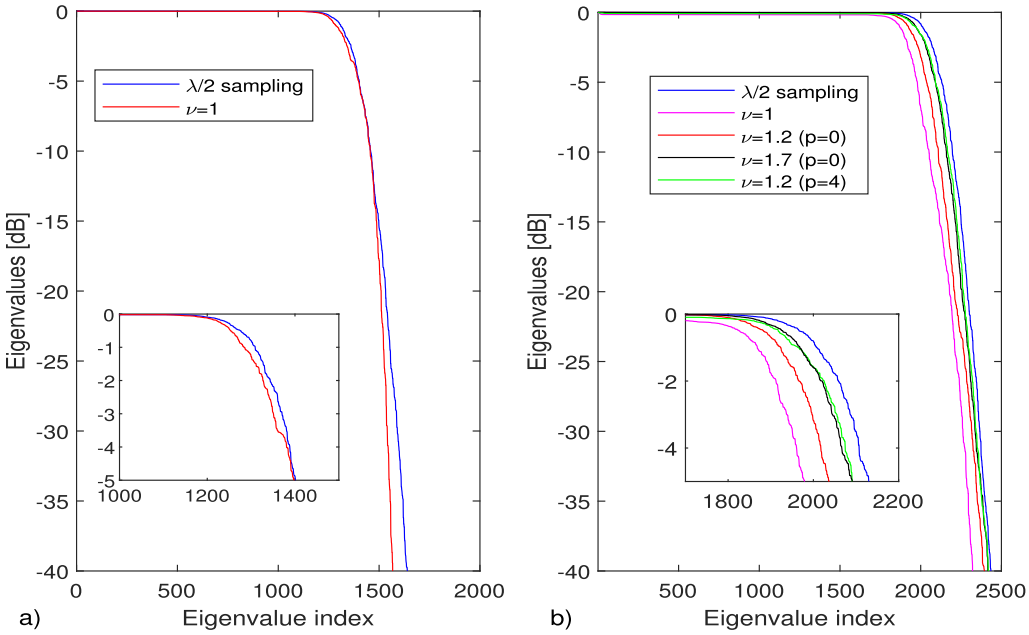

FIGURE 4. Eigenvalue estimation of $\mathcal{G}\mathcal{G}^{\dagger}$ for $X_s = Y_s = 13.78\lambda$ and $z_o = 8.2\lambda$. Panel a) refers to the case $OD = SD$ whereas panel b) to the case $X_0 = Y_0 = 25.1\lambda$.

$N_{\lambda/2} = 10404$ points. As can be seen, the uniform oversampling with $\nu = 1$ and $\nu = 1.2$ requires much fewer samples than $N_{\lambda/2}$ (i.e., $N_{\nu=1} = 2809$ and $N_{\nu=1.2} = 3969$) but fail to approximate well the eigenvalues until the oversampling factor reaches $\nu = 1.7$, for which $N_{\nu=1.7} = 7981$. Therefore, in these cases the data saving allowed by the uniform oversampling strategy is strongly reduced. Instead, the same level of accuracy in predicting the eigenvalues as the uniform oversampling for $\nu = 1.7$ is already reached by the proposed non-uniform oversampling strategy for $\nu = 1.2$ and by setting $p = 4$. Since, the number of sampling points depends only on ν, the non-uniform oversampling requires 3969 measurement points instead of 7981 required by the warping uniform sampling. Moreover, such a number is much lower than $N_{\lambda/2}$; indeed, more than 60% of measurement points are saved.

B. RADIATION PATTERN EVALUATION

In this section, we check the proposed sampling strategy for radiation pattern evaluation.

To this end, a planar array enclosed within a square domain $SD = [-X_s, X_s] \times [Y_s, Y_s]$ is considered, with $X_s = Y_s = 13.78\lambda$, whereas the measurement aperture is $OD = [-X_O, X_O] \times [Y_O, Y_O]$ with $X_O = Y_O = 25.1\lambda$. Note that this is exactly the same case addressed in the previous numerical example concerning the eigenvalue computation.

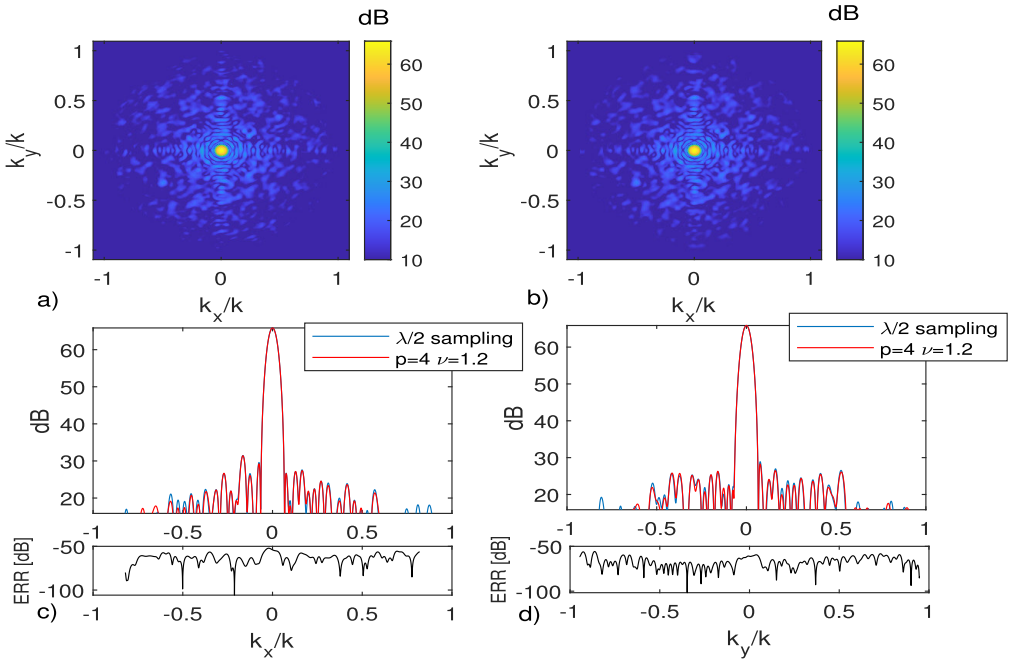

FIGURE 5. Amplitude of the sum radiation pattern for the broad-side direction. In panel a), the radiation pattern is obtained by employing the near-field data according to the proposed non-uniform sampling scheme ($\nu = 1.2, p = 4$) and then interpolated over a $\lambda/2$ grid. In panel b), the radiation pattern is obtained by directly employing the near-field data collected over a uniform $\lambda/2$ grid. Panels c) and d) show the cut-views passing through the main-beam maximum along k_x and k_y, respectively, and the related ERR in dB. The representation errors are $\text{REA}_{\text{dB}} = -31\text{dB}$ and $\text{REP}_{\text{dB}} = -33\text{dB}$.

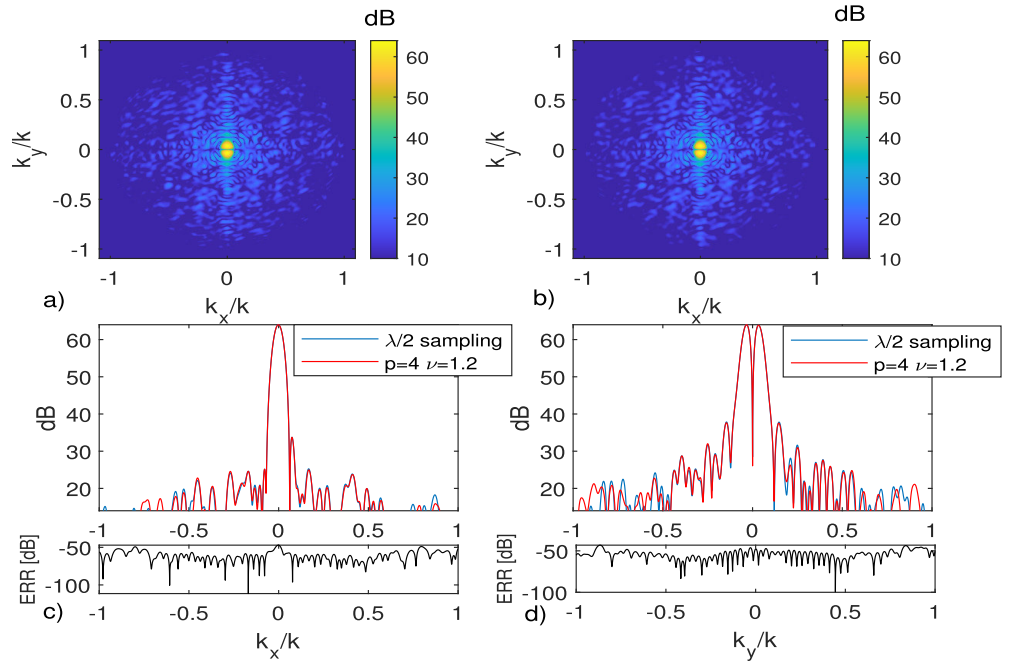

FIGURE 6. Amplitude of the vertical difference radiation pattern for the broad-side direction. In panel a), the radiation pattern is obtained by employing the near-field data according to the proposed non-uniform sampling scheme ($\nu = 1.2, p = 4$) and then interpolated over a $\lambda/2$ grid. In panel b), the radiation pattern is obtained by directly employing the near-field data collected over a uniform $\lambda/2$ grid. Panels c) and d) show the cut-views passing through the main-beam maximum along k_x and k_y, respectively, and the related ERR in dB. The representation errors are $\text{REA}_{\text{dB}} = -29\text{dB}$ and $\text{REP}_{\text{dB}} = -31\text{dB}$.

Available near-field data refer to a multi-beam tracking radar system able to radiate both sum, difference-over azimuth and difference-over elevation patterns. The main y linear component of the near-field has been provided at a

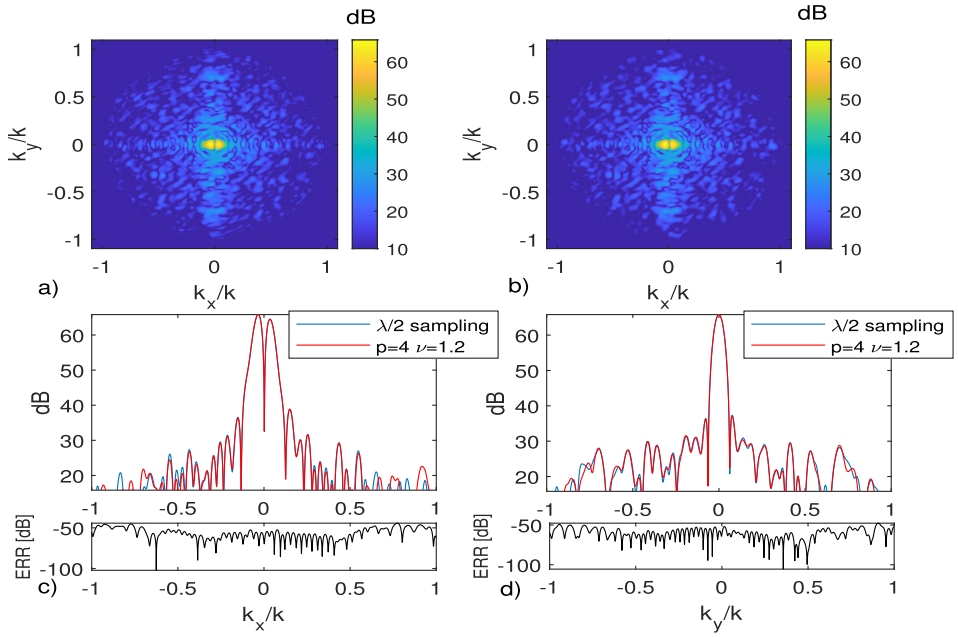

FIGURE 7. Amplitude of the horizontal difference radiation pattern for the broad-side direction. In panel a), the radiation pattern is obtained by employing the near-field data according to the proposed non-uniform sampling scheme ($\nu = 1.2, p = 4$) and then interpolated over a $\lambda/2$ grid. In panel b), the radiation pattern is obtained by directly employing the near-field data collected over a uniform $\lambda/2$ grid. Panels c) and d) show the cut-views passing through the main-beam maximum along k_x and k_y, respectively, and the related ERR in dB. The representation errors are $\text{REA}_{\text{dB}} = -29\text{dB}$ and $\text{REP}_{\text{dB}} = -31\text{dB}$.

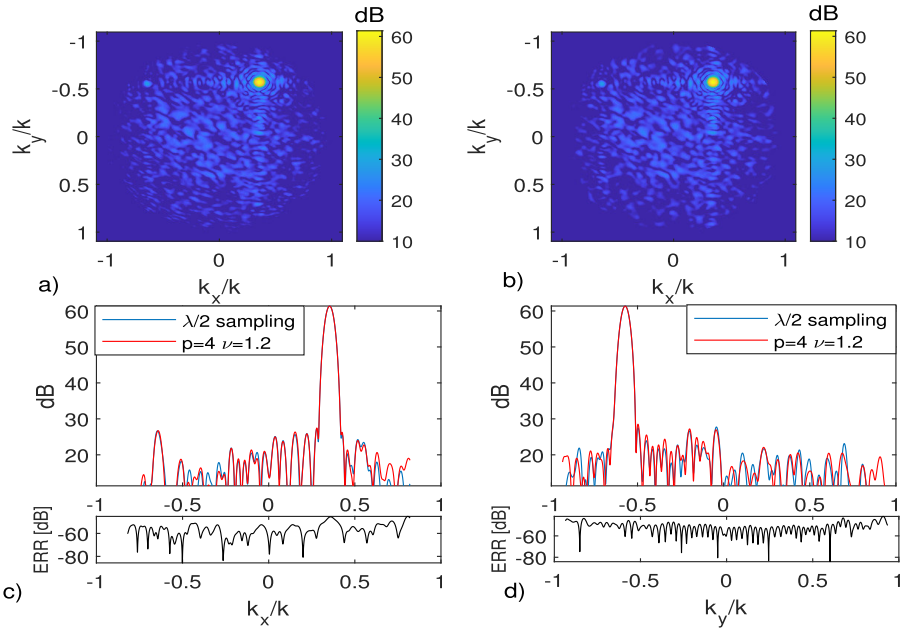

FIGURE 8. Amplitude of the sum radiation pattern for the steering direction $(\phi_s, \theta_s) = (-58.3°, 42.2°)$. In panel a), the radiation pattern is obtained by employing the near-field data according to the proposed non-uniform sampling scheme ($\nu = 1.2, p = 4$) and then interpolated over a $\lambda/2$ grid. In panel b), the radiation pattern is obtained by directly employing the near-field data collected over a uniform $\lambda/2$ grid. Panels c) and d) show the cut-views passing through the main-beam maximum along k_x and k_y, respectively, and the related ERR in dB. The representation errors are $\text{REA}_{\text{dB}} = -23\text{dB}$ and $\text{REP}_{\text{dB}} = -25\text{dB}$.

single frequency and taken at the usual $\lambda/2$ step. Therefore, measurements taken at the required non-uniform step were not actually available. To mimic the non-uniform sampling, data collected under the mentioned uniform sampling are first interpolated and then re-sampled over the required non-uniform grid. Of course, this last step is not required if the measurement set-up is since the outset set to comply with the non-uniform sampling. Moreover, this further step is not

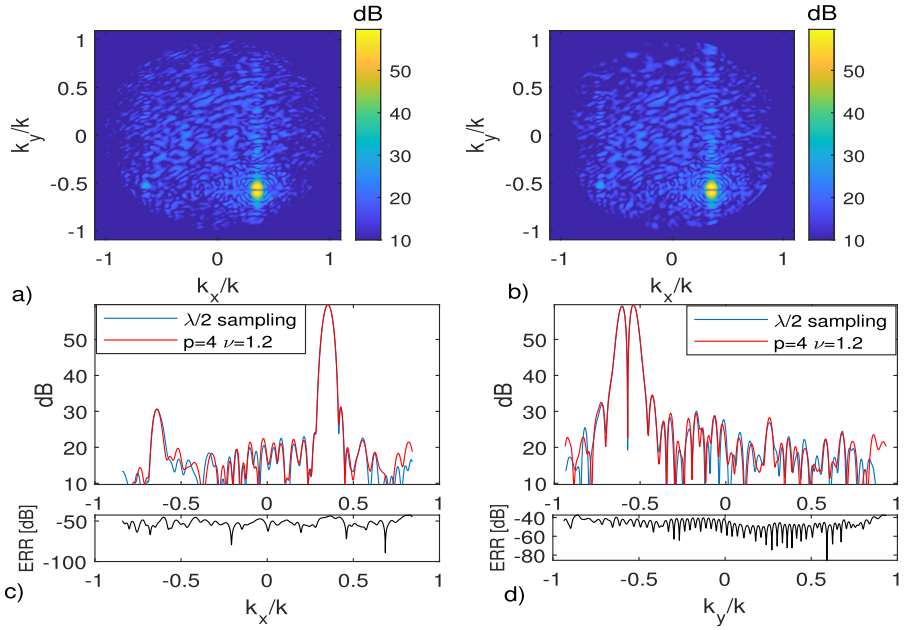

FIGURE 9. Amplitude of the vertical difference radiation pattern for the steering direction $(\phi_S, \theta_S) = (-58.3°, 42.2°)$. In panel a), the radiation pattern is obtained by employing the near-field data according to the proposed non-uniform sampling scheme ($\nu = 1.2, p = 4$) and then interpolated over a $\lambda/2$ grid. In panel b), the radiation pattern is obtained by directly employing the near-field data collected over a uniform $\lambda/2$ grid. Panels c) and d) show the cut-views passing through the main-beam maximum along k_x and k_y, respectively, and the related ERR in dB. The representation errors are $\text{REA}_{\text{dB}} = -20\text{dB}$ and $\text{REP}_{\text{dB}} = -22\text{dB}$.

an advantage for the non-uniform sampling since further interpolation error could be added.

The radiation pattern has been then obtained by Fourier transforming the measured field component. More in detail, the radiation patterns are shown as functions of the spectral variables $k_x = k \sin\theta \cos\phi$ and $k_y = k \sin\theta \sin\phi$, with θ and ϕ being the usual polar angles, and shown within the so-called visible domain, that is for $k_x^2 + k_y^2 \leq k^2$. Also, according to the arguments showed in the previous sections, here we only compare the radiation pattern obtained by the $\lambda/2$ sampling and the ones returned by the warping method with non-uniform oversampling of parameters $\nu = 1.2$ and $p = 4$.. Hence, the corresponding data reduction is the same as highlighted above.

It must be noted that, while the half-wavelength sampling already returns data suited for FFT, the non-uniform sampling requires the data to be first interpolated (according to (19)) over a uniform $\lambda/2$ grid. We denote as $E_{\lambda/2}$ the near-field data directly collected over the uniform $\lambda/2$ grid and as E_ν^p the field collected according to the non-uniform sampling scheme (actually, re-sampled on the non-uniform grid), of parameter ν and p, and then interpolated over a $\lambda/2$ uniform grid by (19).

In order to compare the two different sampling strategies, we consider different error metrics. The first one measures the representation error over the aperture and is defined as

$$\text{REA}_{\text{dB}}(X_0, Y_0, \nu, p) = 20 \log_{10} \frac{||E_\nu^p - E_{\lambda/2}||}{||E_{\lambda/2}||}, \qquad (21)$$

where $\|\cdot\|$ is the Frobenius norm. The second one, is the analogous of (22) referred to the radiation pattern, that is

$$\text{REP}_{\text{dB}}(X_0, Y_0, \nu, p) = 20 \log_{10} \frac{||F_\nu^p - F_{\lambda/2}||}{||F_{\lambda/2}||}, \qquad (22)$$

where F_ν^p and $F_{\lambda/2}$ denote the radiation patterns obtained by the two sampling schemes under comparison. Finally, as a further way to assess the difference between the two sampling schemes we display the punctual error $\text{ERR}(k_x, k_y) = \frac{|F_\nu^p - F_{\lambda/2}|}{|F_{\lambda/2}^{max}|}$, with $F_{\lambda/2}^{max}$ being the maximum of $F_{\lambda/2}$ in the visible domain. This last metrics is suited for the case at hand since the radiation patterns consists basically of a single beam.

We run the comparison for many pointing directions. Herein, for the sake of brevity, we keep showing only a few cases that, however, refer to both the sum and difference beams. Anyway, the results corresponding to other pointing directions show similar quality as the one here reported.

Figs. 5 to 7 show the comparison for the different types of beam under the broad-side direction. As expected, the radiation patterns exhibit a unique focused beam with a very low relative side-lobe level. Moreover, in spite the proposed non-uniform sampling requires less than the 60% samples compared to the standard uniform approach, both the representation error are very low and around -30 dB for all the cases. Also, the radiation patterns show an excellent agreement with the benchmark as can be appreciated by the curves concerning ERR which show the behaviour, along the cut-views, of the

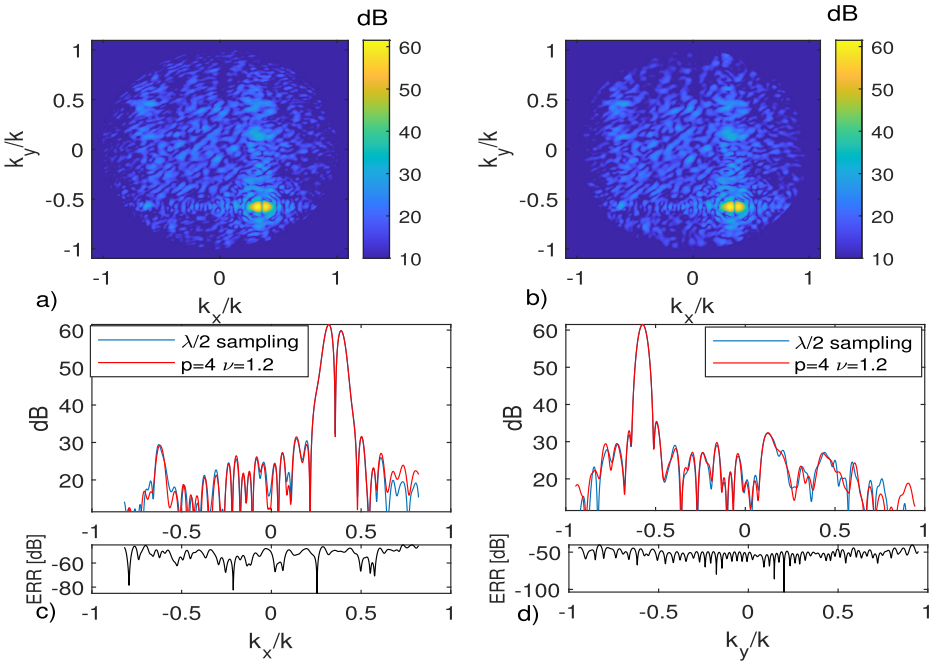

FIGURE 10. Amplitude of the horizontal difference radiation pattern for the steering direction $(\phi_s, \theta_s) = (-58.3°, 42.2°)$. In panel a), the radiation pattern is obtained by employing the near-field data according to the proposed non-uniform sampling scheme ($\nu = 1.2, p = 4$) and then interpolated over a $\lambda/2$ grid. In panel b), the radiation pattern is obtained by directly employing the near-field data collected over a uniform $\lambda/2$ grid. Panels c) and d) show the cut-views passing through the main-beam maximum along k_x and k_y, respectively, and the related ERR in dB. The representation errors are $\text{REA}_{\text{dB}} = -20\text{dB}$ and $\text{REP}_{\text{dB}} = -23\text{dB}$.

normalized local error. As can be seen, this error is much lower the side-lobe level.

Figs. 8 to 10 instead refer to the case the beam is steered at $(\phi_s, \theta_s) = (-58.3°, 42.2°)$. This is a more complex case, compared to the previous one, since the near-field presents relevant projections onto high order singular functions. This is reflected in the representation error (reported once again in the pertinent captions) which actually is increased. Nonetheless, it is still very low, around -20dB. Moreover, the normalized local error is still well below the side-lobes.

Eventually, according to the previous examples, it can be concluded that the proposed near-field sampling scheme allows to achieve performance that is similar to the classical $\lambda/2$ sampling but with a much lower number of measurement points.

V. CONCLUSION

In this paper, the problem of sampling the field radiated by a planar source and observed over a finite planar aperture located in the near-field has been addressed. The problem has been cast as the determination of the measurement spatial positions for which the singular values of the radiation operator are well-approximated. In particular, in order to determine the sampling points we adopted the warping approach introduced in [23]. More in detail, such an approach has been improved by introducing a spatially varying oversampling strategy. This allowed us to overcome the limitations of the previous version and to deal with measurement apertures that are larger than the source.

The theoretical arguments have been validated by numerical experiment based examples. It was shown that the proposed approach retains almost the same quality as the classical $\lambda/2$ sampling but requires much fewer measurement points. For the considered examples, more than 60% of the sampling points were saved.

As future developments, our commitments concern different directions. One is the expansion of the theory in order to find more general warping transformations that allow to rigorously deal with the cases addressed herein. Also, it is of sure interest to consider the cases when the radiation system is not planar [28] or amplitude only measurements are available [29].

ACKNOWLEDGMENT

The authors kindly thank Giuseppina Nuzzo for proofreading the manuscript.

REFERENCES

[1] A. Yaghjian, "An overview of near-field antenna measurements," *IEEE Trans. Antennas Propag.*, vol. AP-34, no. 1, pp. 30–45, Jan. 1986.

[2] M. H. Francis and R. W. Wittmann, "Near-field scanning measurements: Theory and practice," in *Modern Antenna Handbook*, C. A. Balanis, Ed. Hoboken, NJ, USA: Wiley, 2008, pp. 929–976.

[3] W. Leach and D. Paris, "Probe compensated near-field measurements on a cylinder," *IEEE Trans. Antennas Propag.*, vol. AP-21, no. 4, pp. 435–445, Jul. 1973.

[4] O. Breinbjerg, "Spherical near-field antenna measurements—The most accurate antenna measurement technique," in *Proc. IEEE Int. Symp. Antennas Propag. (APSURSI)*, Fajardo, Puerto Rico, Jun. 2016, pp. 1019–1020.

[5] F. Rodriguez Varela, B. G. Iraguen, and M. Sierra-Castaner, "Near-field to far-field transformation on arbitrary surfaces via multi-level spherical wave expansion," *IEEE Trans. Antennas Propag.*, vol. 68, no. 1, pp. 500–508, Jan. 2020.
[6] C. H. Schmidt and T. F. Eibert, "Multilevel plane wave based near-field far-field transformation for electrically large antennas in free-space or above material halfspace," *IEEE Trans. Antennas Propag.*, vol. 57, no. 5, pp. 1382–1390, May 2009.
[7] T. B. Hansen and A. D. Yaghjian, *Plane-Wave Theory of Time-Domain Fields: Near-Field Scanning Applications*. Hoboken, NJ, USA: Wiley-IEEE Press, 1999.
[8] F. Dagostino, F. Ferrara, C. Gennarelli, R. Guerriero, and M. Migliozzi, "Fast and accurate far-field prediction by using a reduced number of bipolar measurements," *IEEE Antennas Wireless Propag. Lett.*, vol. 16, pp. 2939–2942, 2017.
[9] M. Migliore, "Near field antenna measurement sampling strategies: From linear to nonlinear interpolation," *Electronics*, vol. 7, no. 10, p. 257, Oct. 2018.
[10] A. Capozzoli, C. Curcio, A. Liseno, and P. Vinetti, "Field sampling and field reconstruction: A new perspective," *Radio Sci.*, vol. 45, no. 6, pp. 1–31, Dec. 2010.
[11] R. Piestun and D. A. B. Miller, "Electromagnetic degrees of freedom of an optical system," *J. Opt. Soc. Amer. A, Opt. Image Sci.*, vol. 17, no. 5, pp. 892–902, 2000.
[12] M. D. Migliore, "On electromagnetics and information theory," *IEEE Trans. Antennas Propag.*, vol. 56, no. 10, pp. 3188–3200, Oct. 2008.
[13] A. J. Jerri, "The Shannon sampling theorem—Its various extensions and applications: A tutorial review," *Proc. IEEE*, vol. 65, no. 11, pp. 1565–1596, Nov. 1977.
[14] R. Solimene, M. A. Maisto, and R. Pierri, "Inverse source in the near field: The case of a strip current," *J. Opt. Soc. Amer. A, Opt. Image Sci.*, vol. 35, no. 5, pp. 755–763, 2018.
[15] G. G. Lorentz, "Metric entropy and approximation," *Bull. Amer. Math. Soc.*, vol. 72, no. 6, pp. 903–937, 1966.
[16] S. J. Reeves and L. P. Heck, "Selection of observations in signal reconstruction," *IEEE Trans. Signal Process.*, vol. 43, no. 3, pp. 788–791, Mar. 1995.
[17] S. Joshi and S. Boyd, "Sensor selection via convex optimization," *IEEE Trans. Signal Process.*, vol. 57, no. 2, pp. 451–462, Feb. 2009.
[18] J. Ranieri, A. Chebira, and M. Vetterli, "Near-optimal sensor placement for linear inverse problems," *IEEE Trans. Signal Process.*, vol. 62, no. 5, pp. 1135–1146, Mar. 2014.
[19] C. Jiang, Y. C. Soh, and H. Li, "Sensor placement by maximal projection on minimum eigenspace for linear inverse problems," *IEEE Trans. Signal Process.*, vol. 64, no. 21, pp. 5595–5610, Nov. 2016.
[20] A. Capozzoli, C. Curcio, and A. Liseno, "Truncation in 'quasi-raster' near-field acquisitions [measurements corner]," *IEEE Antennas Propag. Mag.*, vol. 54, no. 5, pp. 174–183, Oct. 2012.
[21] A. Capozzoli, L. Celentano, C. Curcio, A. Liseno, and S. Savarese, "Twice optimised near-field scanning system for antenna characterisation," *IET Microw., Antennas Propag.*, vol. 14, no. 3, pp. 163–173, Feb. 2020.
[22] O. M. Bucci, C. Gennarelli, and C. Savarese, "Representation of electromagnetic fields over arbitrary surfaces by a finite and nonredundant number of samples," *IEEE Trans. Antennas Propag.*, vol. 46, no. 3, pp. 351–359, Mar. 1998.
[23] M. Maisto, R. Pierri, and R. Solimene, "Near-field warping sampling scheme for broad-side antenna characterization," *Electronics*, vol. 9, no. 6, p. 1047, Jun. 2020.
[24] M. D. Migliore, "On the role of the number of degrees of freedom of the field in MIMO channels," *IEEE Trans. Antennas Propag.*, vol. 54, no. 2, pp. 620–628, Feb. 2006.
[25] K. Khare, "Sampling theorem, bandlimited integral kernels and inverse problems," *Inverse Problems*, vol. 23, no. 4, pp. 1395–1416, Aug. 2007.
[26] R. Solimene, M. A. Maisto, and R. Pierri, "Sampling approach for singular system computation of a radiation operator," *J. Opt. Soc. Amer. A, Opt. Image Sci.*, vol. 36, no. 3, pp. 353–361, 2019.
[27] K. Horiuchi, "Sampling principle for continuous signals with time-varying bands," *Inf. Control*, vol. 13, no. 1, pp. 53–61, Jul. 1968.
[28] G. Leone, F. Munno, and R. Pierri, "Inverse source on conformal conic geometries," *IEEE Trans. Antennas Propag.*, vol. 69, no. 3, pp. 1596–1609, Mar. 2021, doi: 10.1109/TAP.2020.3016375.
[29] R. Moretta and R. Pierri, "Performance of phase retrieval via phaselift and quadratic inversion in circular scanning case," *IEEE Trans. Antennas Propag.*, vol. 67, no. 12, pp. 7528–7537, Dec. 2019.

MARIA ANTONIA MAISTO received the M.S. degree *(summa cum laude)* in electronic engineering and the Ph.D. degree in electronic and computer science engineering from the University of Campania Luigi Vanvitelli, Aversa, Italy, in 2012 and 2015, respectively. Since 2016, she has been holding a postdoctoral fellowship with the Department of Engineering, Universitá degli Studi della Campania Luigi Vanvitelli. Her current research interest includes electromagnetic inverse problems with particular attention to theoretical and numerical aspects, in particular, electromagnetic inverse source and inverse scattering problems, electromagnetic field information content, microwave radar imaging, RCS estimation from near-field measurements, and electromagnetic field sampling.

GIOVANNI LEONE (Member, IEEE) received the Laurea degree in electronic engineering from the University of Naples Federico II, Naples, Italy, in 1981. From 1986 to 1992, he was an Associate Researcher of electromagnetics with the University of Salerno, Italy. From 1992 to 2000, he was an Associate Professor with the University of Salerno and the Seconda Universitá degli Studi di Napoli, Italy. He is currently a Full Professor with the University of Campania Luigi Vanvitelli, Italy. He was responsible for research funding from the Italian Space Agency, Rome, Italy, the National Research Council, and the Ministry of Scientific Research. His current research interests include antenna measurement techniques and synthesis, phase retrieval of radiated fields, inverse scattering for nondestructive diagnostics, microwave tomography for subsurface sensing, and conformal antennas diagnostics.

ADRIANA BRANCACCIO (Member, IEEE) received the Ph.D. degree (Hons.) in electronic engineering from the University of Napoli Federico II, in 1994. She is currently an Associate Professor of electromagnetic fields with the University of Campania Luigi Vanvitelli. Her scientific activities are in the field of inverse electromagnetic scattering, with contributions on mathematical models and on the applications, and with verification of both simulated and experimental data. Her main research interests include the non-destructive diagnosis of masonry, the tomographic processing of georadar data for subsurface prospecting, and the localization and shape reconstruction of metallic and dielectric objects.

RAFFAELE SOLIMENE (Senior Member, IEEE) received the Laurea *(summa cum laude)* and Ph.D. degrees in electronic engineering from the Seconda Universitá degli Studi di Napoli (SUN), Aversa, Italy, in 1999 and 2003, respectively. In 2002, he became an Assistant Professor with the Faculty of Engineering, Mediterranea University of Reggio Calabria, Italy. Since 2006, he has been with the Dipartimento di Ingegneria, University of Campania Luigi Vanvitelli, where he is currently an Associate Professor. Based on the following topics, he has coauthored more than 250 scientific works. His research interests include inverse electromagnetic problems with applications to inverse source and array diagnostics, non-destructive subsurface investigations, through-the-wall and GPR imaging, and breast cancer detection. On these topics, he routinely serves as a reviewer for a number of journals, and organized several scientific sessions. He is also an Associate Editor for four scientific journal, among which IEEE Geoscience and Remote Sensing Letters.